Traffic 2006; 7: 524–537
Blackwell Munksgaard

doi: 10.1111/j.1600-0854.2006.00403.x

Effects of Dynactin Disruption and Dynein Depletion on Axonal Microtubules

Fridoon J. Ahmad[1,2,a], Yan He[1,a], Kenneth A. Myers[1], Thomas P. Hasaka[1], Franto Francis[3], Mark M. Black[3] and Peter W. Baas[1,*]

[1]*Department of Neurobiology and Anatomy, Drexel University College of Medicine, Philadelphia, PA, USA*
[2]*Centre for Excellence Molecular Biology, University of the Punjab, Pakistan*
[3]*Department of Anatomy and Cell Biology, Temple University School of Medicine, Philadelphia, PA, USA*
** Corresponding author: Peter W. Baas, pbaas@drexelmed.edu*

We investigated potential roles of cytoplasmic dynein in organizing axonal microtubules either by depleting dynein heavy chain from cultured neurons or by experimentally disrupting dynactin. The former was accomplished by siRNA while the latter was accomplished by overexpressing P50-dynamitin. Both methods resulted in a persistent reduction in the frequency of transport of short microtubules. To determine if the long microtubules in the axon also undergo dynein-dependent transport, we ascertained the rates of EGFP-EB3 "comets" observed at the tips of microtubules during assembly. The rates of the comets, in theory, should reflect a combination of the assembly rate and any potential transport of the microtubule. Comets were intitally slowed during P50-dynamitin overexpression, but this effect did not persist beyond the first day and was never observed in dynein-depleted axons. In fact, the rates of the comets were slightly faster in dynein-depleted axons. We conclude that the transient effect of P50-dynamitin overexpression reflects a reduction in microtubule polymerization rates. Interestingly, after prolonged dynein depletion, the long microtubules were noticeably misaligned in the distal regions of axons and failed to enter the filopodia of growth cones. These results suggest that the forces generated by cytoplasmic dynein do not transport long microtubules, but may serve to align them with one another and also permit them to invade filopodia.

Key words: axon, cytoplasmic dynein, dynactin, EB3, microtubule, neurofilament, neuron

Received 9 November 2005, revised and accepted for publication 30 January 2006, published on-line 17 March 2006

Microtubules are critical cytoskeletal components within the axon. They are aligned into a paraxial bundle that extends from the cell body into the growth cone. In the peripheral region of the growth cone, the microtubule bundle splays apart so that individual microtubules can invade filopodia (1). Within the bundle, some microtubules can achieve lengths exceeding 100 μm, while other microtubules are quite short, only a few microns in length (2,3). Recent photobleach-based live-cell imaging studies have established that short microtubules undergo rapid concerted transport within the axons of cultured neurons (4–6). Roughly two-thirds of these short microtubules, which are generally no longer than 7 μm, are transported anterogradely, while the rest are transported retrogradely. Interestingly, these studies failed to detect any movement of the longer microtubules.

A few years ago, we sought to determine whether cytoplasmic dynein is a principal motor for transporting microtubules within axons. For these studies, we microinjected recombinant P50-dynamitin into cultured neurons. P50-dynamitin is one component of the dynactin complex, which is thought to be important for dynein-based functions. Excess P50-dynamitin causes the dynactin complex to dissociate, thereby compromising dynein functions (7). We found that injection of P50-dynamitin suppressed the outward relocation of microtubules from the centrosome into the axon (8). On this basis, we concluded that cytoplasmic dynein is indeed a critical motor for transporting microtubules, at least in the outward direction. Recently, we were able to test the role of cytoplasmic dynein in the transport of axonal microtubules in a more direct manner using the photobleach approach on cultured neurons depleted of dynein heavy chain (DHC) with siRNA (6). We found that the frequency of the anterograde transport of microtubules was halved, while their retrograde transport was unaffected. These results confirm that a significant portion of the anterograde transport of short microtubules in the axon is fueled by cytoplasmic dynein.

The question arises as to whether cytoplasmic dynein distinguishes short microtubules from long microtubules, or alternatively, whether the same forces are generated on microtubules irrespective of their length. Ma *et al.* (9) recently surmised that the potential transport of the long microtubules could be studied by measuring the velocities of comets produced at the plus ends of the microtubules when expressing EGFP-fusions with +TIPs, a category of protein that associates with the plus ends of microtubules as they assemble. These authors reasoned that the velocity of the comet should exceed known rates of microtubule polymerization, if the microtubules were undergoing transport. No comets were observed to move at such a rate, and hence it was tentatively concluded that long microtubules are stationary. However, microtubule polymerization and transport rates

[a]These authors contributed equally and should be considered as co-first authors.

can certainly vary (10), and hence these observations do not exclude the possibility that molecular motors could produce short tugs of movement on these microtubules.

In the present study, we sought to evaluate the role of dynein-driven forces in the transport and organization of axonal microtubules, both long and short. We used two different approaches for suppressing dynein function, the siRNA-based approach of depleting DHC and dynactin disruption via overexpression of excess P50-dynamitin. In order to perform these two approaches in parallel, we overexpressed P50-dynamitin rather than injecting recombinant protein. Our primary goal was to understand whether dynein-driven forces transport the longer microtubules, and if not, whether these forces play a different role in the configuration of the long microtubules. Another goal was to better understand the effects of dynactin disruption, given recent studies showing that dynactin can potentially interact with a broad array of motor and non-motor proteins in addition to cytoplasmic dynein (11).

Results

Inhibition of dynein-related functions by overexpression of P50-dynamitin in cultured sympathetic neurons

Disruption of the dynactin complex by introducing excess P50-dynamitin into cells is a common method for experimentally inhibiting dynein functions (7,8,11–13). We previously reported that an acute microinjection (at high concentrations) of recombinant P50-dynamitin into cultured neurons is profoundly deleterious to axonal outgrowth (8). Here we determined the effects of overexpressing the protein, which is a more common approach than microinjecting it. We found that an overnight bout of overexpression of P50-dynamitin did not curtail the outgrowth of axons (Figure 1). Axons were similar in length to axons from control neurons expressing myc-tag alone. This was also the case when neurons were permitted to overexpress the construct for 2–4 days, after which they were re-plated and allowed to grow axons a second time.

The lack of inhibition of axonal growth may relate to the fact that the protein levels we are able to achieve with the overexpression approach are not as high as the levels obtained by microinjection. In addition, an acute introduction of the protein may produce more dramatic effects than a gradual accumulation of the protein. Many of the neurons overexpressing P50-dynamitin displayed axons with blunt swollen tips (Figure 1D), which is consistent with a distal accumulation of organelles that would be expected with the inhibition of cytoplasmic dynein. At the immunofluorescence level, it was not uncommon for microtubules to appear slightly more splayed, particularly in their thickened distal regions and at branch points (Figure 1E). The microtubule array was otherwise similar to that of control axons, and the staining for filamentous actin was indistinguishable from controls (not shown).

Before analyzing the microtubule array in finer detail, we wished to further confirm that the dynein-related functions were at least partially compromised. For this, we

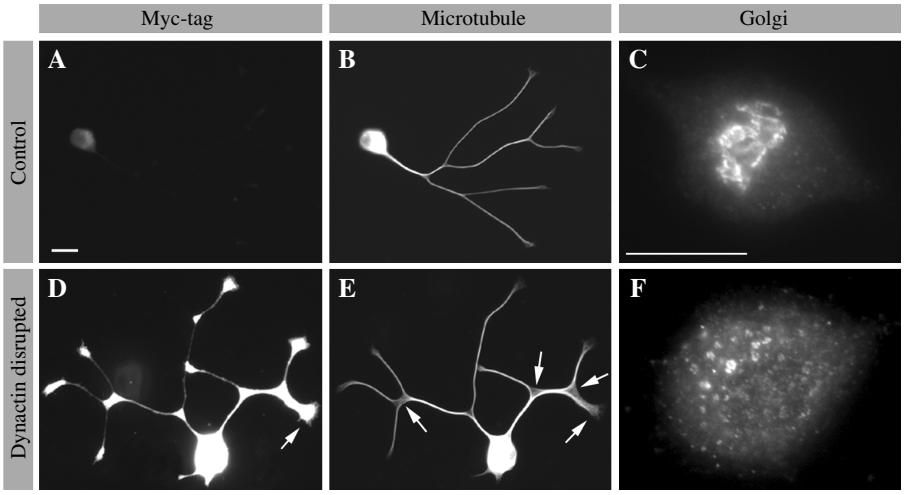

Figure 1: Axonal morphology and Golgi dispersion in cultured rat sympathetic neurons as a result of dynactin disruption. Panels A and D show a control neuron and P50-dynamitin-myc-expressing neuron (high expresser), respectively, stained with an antibody to myc. Shown here is a control neuron that was not transfected for myc, but for quantitative analyses, we routinely used control neurons transfected to express the myc-tag. Immunofluorescence labeling for tubulin reveals microtubule organization within the control (B) and experimental (E) neuron. Note that the distal regions of the axons and the branching regions of the P50-dynamitin-myc-expressing neurons are sometimes thickened, with microtubules somewhat more splayed apart compared to controls (see arrows). Golgi apparatus morphologies labeled by Golgi-58K protein immunostaining revealed compact, center-located Golgi apparatus in a control neuron (C), and fragmented and dispersed Golgi in a P50-dynamitin-myc-expressing neuron (F). Scale bars, 20 μm.

examined the distribution of Golgi elements and neurofilaments, both of which are thought to depend on cytoplasmic dynein for their distribution. Cytoplasmic dynein is known to be the principal motor for transporting organelles toward the minus ends of microtubules (13,14), a function which moves organelles from the axonal tip back to the cell body and which compresses Golgi elements into their typical perinuclear locale (15). In cultured sympathetic neurons, the intact Golgi apparatus appears as a compact, multitubular structure located near the cell center (Figure 1C). However, in neurons overexpressing P50-dynamitin, the Golgi apparatus was fragmented and dispersed throughout the cytoplasm (Figure 1F), which is similar to the effect observed in non-neuronal cells overexpressing P50-dynamitin (16). All non-neuronal cells in the cultures that highly expressed the construct displayed a dispersed Golgi apparatus on the first day after transfection (data not shown). In contrast, only 24% of the highly expressing neurons revealed dispersed Golgi at 24 h post-transfection. This proportion increased to 57 and 66% at 48 and 72 h post-transfection, respectively.

In control neurons, neurofilaments were distributed along the length of the axon, with the previously reported 'natural gaps' throughout the axon (17–19). In some cases there was a slight enrichment of neurofilaments in the proximal regions (Figure 2A). In contrast, the neurons expressing P50-dynamitin-myc showed a dramatic accumulation of neurofilaments in the most distal several microns of the axon, and a corresponding decrease proximally (Figure 2B; see Figure 2C for quantitative analysis). Neurofilament staining intensity for the entire axon was quantified as was staining intensity for the proximal and distal 10% of the axon. The staining intensities in the proximal and distal 10% of the axon were divided by that for the entire axon to obtain a measure of the relative amount of axonal neurofilaments in these axonal regions. The relative amounts of neurofilaments in the distal axon were 0.09 ± 0.08 and 0.40 ± 0.17 in control and P50-dynamitin-overexpressing neurons, respectively. The relative amounts of neurofilaments in the proximal axon were 0.20 ± 0.08 and 0.08 ± 0.06 in control and P50-dynamitin-overexpressing neurons, respectively. Analyses on the population of axons studied revealed that these differences are statistically significant ($p < 0.0001$ distal, $p < 0.002$ proximal, *t*-test). These results, which are similar to those reported for peripherin intermediate filaments in PC12 cells overexpressing P50-dynamitin (20), were consistently observed with all of the neurons overexpressing P50-dynamitin, even after the first day of plating. These results are also essentially the same as those obtained in our earlier study in which DHC was depleted from sympathetic neurons using siRNA (6) and are consistent with the conclusion that cytoplasmic dynein transports neurofilaments retrogradely but not anterogradely in the axon.

A proportion of the anterograde microtubule transport is inhibited by dynactin disruption

To assay axonal microtubule transport we used our modification (5,6) of the photobleach approach of Wang and Brown (4) (Figure 3A). We previously reported that depletion of DHC by siRNA reduced the frequency of anterograde transport of short microtubules by approximately 50% while having no effect on their retrograde transport frequency (6). Here we wished to ascertain the effects of P50-dynamitin overexpression. Cultured neurons expressing EGFP-tubulin and either a myc-tagged control vector

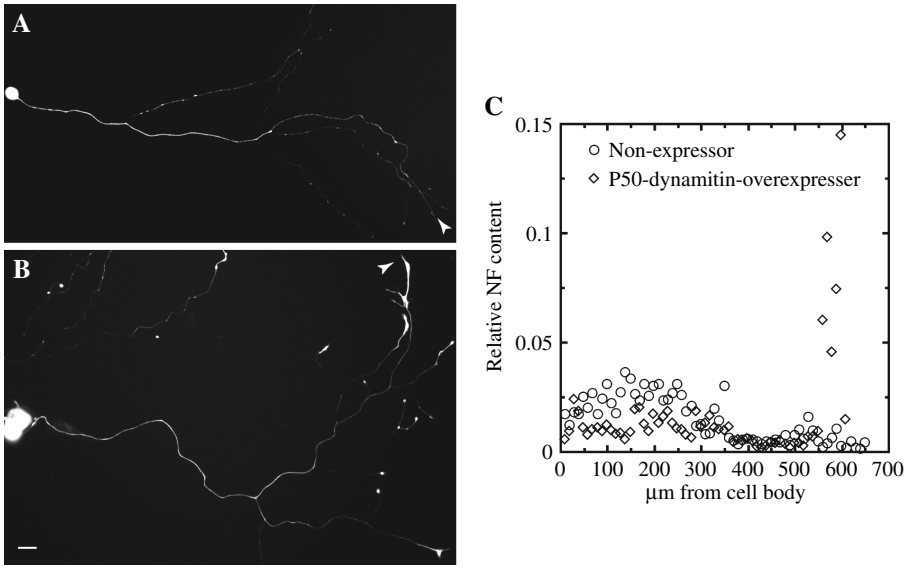

Figure 2: P50-dynamitin overexpression results in marked redistribution of axonal neurofilaments. Panels A and B show neurofilament staining in a control neuron (A) and a neuron overexpressing P50-dynamitin (B). The scale bar represents 19 μm. Panel C shows quantitative analyses of neurofilament staining intensity along the length of the axons indicated by arrowheads in panels A and B. Note the dramatic accumulation of neurofilaments in the distal axon of the P50-dynamitin overexpresser compared to the control and the relatively lower neurofilament staining in the proximal axon of the overexpresser compared to the control. Similar analyses on the population of axons studied revealed that these differences are consistent and statistically significant.

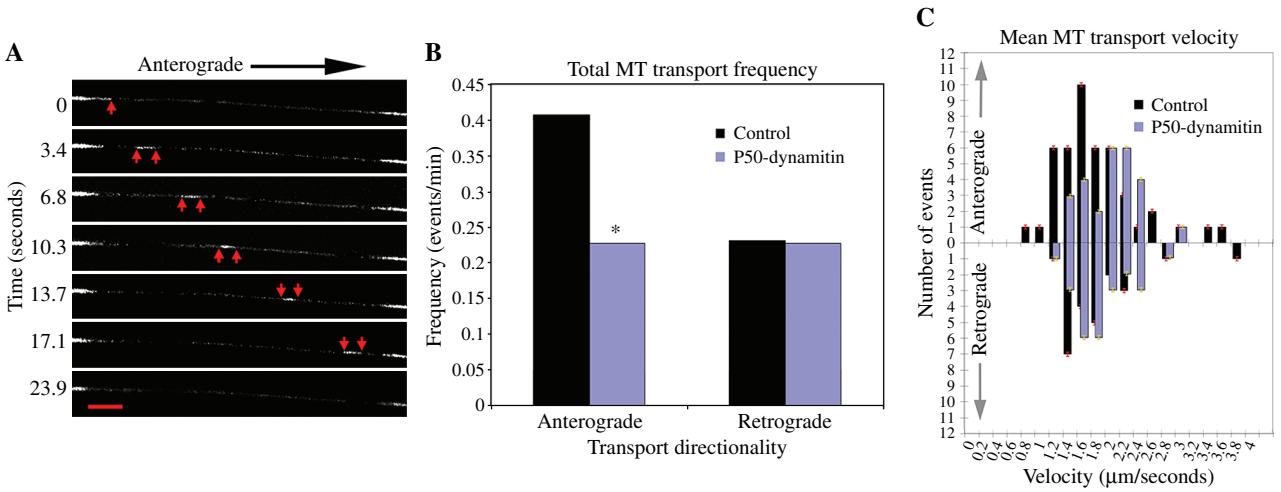

Figure 3: P50-dynamitin overexpression reduces anterograde microtubule transport frequency. (A) Time-lapse images reveal a microtuble moving in the anterograde direction through the photobleached region. Red arrows mark the leading and trailing ends of the microtubule. Subsequent staining for myc confirmed that this axon was from a neuron overexpressing P50-dynamitin. (B) The frequency (events/min) of anterograde microtubule transport was significantly reduced in the axons of P50-dynamitin-myc-expressing neurons (chi-square test, *, $p < 0.001$) as compared to control axons, with no significant difference observed in retrograde transport frequency (chi-square test, $p > 0.05$). (C) Histogram depicting the mean velocities of microtubule movements in the axons of control [velocity $\pm$ SEM $= 1.70 \pm 0.105$ μm/second (anterograde); 1.70 ± 0.116 μm/second (retrograde)] and P50-dynamitin-myc-expressing neurons [velocity $\pm$ SEM $= 1.90 \pm 0.098$ μm/second (anterograde); 1.77 ± 0.103 μm/second (retrograde)]. Comparison of these two groups showed no statistically significant variation in microtubule transport velocity regardless of movement directionality (two-tailed *t*-test, anterograde $p > 0.05$, retrograde $p > 0.05$).

or P50-dynamitin-myc were re-plated (see *Materials and Methods*) 2 days post-transfection and allowed to extend axons over a 16–32-h period of time before performing the microtubule transport assay. Re-plating times were chosen to coincide with earlier studies utilizing the time frame during which siRNA was shown to have substantially reduced cellular levels of DHC (6). There was no apparent difference in axonal length between control and experimental cells under these conditions. In control neurons expressing the myc-tag, transport of microtubules occurred at an anterograde:retrograde ratio of approximately 2:1, with an average 0.409 transport events/min in the anterograde direction, and 0.231 events/min in the retrograde direction. This is consistent with the transport frequencies recorded in control neurons expressing EGFP-tubulin alone (data not shown) as well as control siRNA frequencies previously reported (6). When the transport assay was carried out in P50-dynamitin-overexpressing neurons, there was a dramatic and statistically significant decrease ($p < 0.001$, chi-square test) in the anterograde frequency of microtubule transport, but no change was observed in the frequency of retrograde movements (anterograde $= 0.228$; retrograde $= 0.228$ events/min) (Figure 3B). Further analysis of microtubule transport velocity revealed no statistical difference between control [velocity $\pm$ SEM $= 1.70 \pm 0.105$ μm/second (anterograde); 1.70 ± 0.116 μm/second (retrograde)] and P50-dynamitin-overexpressing neurons [velocity $\pm$ SEM $= 1.90 \pm 0.098$ μm/second (anterograde); 1.77 ± 0.103 μm/second (retrograde)] regardless of transport directionality (anterograde $p > 0.05$; retrograde $p > 0.05$) (Figure 3C). These data are similar to those obtained in our earlier study in which DHC was depleted by siRNA. Taken together with the results on Golgi and neurofilaments, these results suggest that P50-dynamitin overexpression is effective at producing documented effects of dynein depletion.

Effects of dynactin disruption and DHC depletion on microtubule excursions observed with EGFP-EB3

The studies presented thus far suggest that a gradual accumulation of excess P50-dynamitin in the neuron produces similar results to a gradual depletion of DHC, with regard to microtubule transport, neurofilament distribution and Golgi distribution. We next used both the P50-dynamitin approach and the DHC depletion approach to ascertain the potential role of dynein-driven forces on the longer microtubules. To specifically visualize the longer microtubules, we used EGFP-EB3 to study the plus ends of microtubules during bouts of assembly (5,21), given that that short mobile microtubules do not appear to undergo any assembly during their movement (4–6). EB3 is one member of a category of proteins called +TIPs that associate with microtubule plus ends during assembly [for review, see (22)]. The excursion of the EGFP-EB3 at the plus end of the microtubule appears as a moving 'comet' because of the gradual dissociation of EB3 molecules from the microtubule as it continues to add more subunits (thus producing a comet-shaped burst of fluorescence with its tail toward the minus end of the microtubule). In theory, the rates of the EB3

comets should reflect the combined rates of microtubule polymerization and any potential movement of the microtubule (9,23).

We initially performed studies on neurons overexpressing P50-dynamitin and observed a dramatic reduction in comet velocity on the first day of overexpression. We pursued this finding in detail to ascertain whether or not the reduction in comet velocity reflected a diminution in microtubule movement. In previous studies on EB3 or EB1 excursions in neuronal cells, images were usually captured every 3–4 s (9,21). The Bornens laboratory (23) has pointed out that there are advantages in capturing images every 1 second, which maximizes the ability to follow individual comets with certainty. Also, taking images every few seconds may conceal rapid instantaneous velocities that are not sustained longer than 1 second. We obtained movies of EB3 excursions in various compartments of the neuron, including the cell body, the most proximal 10 μm of the axon, within the main shaft of the axon, and the most distal 10 μm of the axon contiguous with the growth cone. We did so in neurons co-expressing E6FP-EB3 and either P50-dynamitin-myc or myc alone. After imaging, cultures were immunostained for myc, and as with all of the studies reported here, data were derived only from the cells that expressed P50-dynamitin-myc highly.

One of the surprising results obtained in the various studies to date using EB1 or EB3 to visualize microtubule behaviors in axons is that a fraction of the excursions are directed toward the cell body, which seems inconsistent with the results of a number of studies showing that microtubules in axons are uniformly oriented with plus ends distal to the cell body [see for example (24)]. We have observed that the fraction of these retrograde excursions is higher (as high as 15%) during early axogenesis (consistent with observations from the earlier studies) but then diminishes as the axon grows (5). In bona fide axons with lengths on the order of 100 μm, we observed no more than roughly 5% of the excursions in the retrograde direction within the axonal shaft, but higher proportions in the most distal and proximal regions. It is unclear at present (given that the tail of the EGFP-EB3 comet is not so easy to resolve in neurons) whether these retrograde excursions are oppositely oriented microtubules, correctly oriented microtubules whose ends curve backward, or correctly oriented microtubules that are being transported retrogradely. Because of this ambiguity, we chose to exclude the retrograde excursions from the present analyses and focus exclusively on the anterograde excursions. It is worth noting, however, that the P50-dynamitin-myc expression did not detectably alter the proportion of backward to forward comets.

In control neurons expressing myc for 15–20 h, the average EGFP-EB3 excursion velocities for the cell body, proximal axon, main shaft, and distal axon were 0.30 ± 0.10, 0.30 ± 0.10, 0.39 ± 0.10, and 0.39 ± 0.12, μm/second (mean ± SEM), respectively, (Table 1). Figure 4A shows an example from the main shaft. These average velocities are notably faster than in the neurons that had been plated for longer periods of time (see later). The fastest velocities for individual comets (measured over a few seconds time) were on the order of 0.4–0.5 μm/second. When we analyzed instantaneous (second-by-second) velocities, we found that many comets displayed one or more instantaneous velocity that exceeded 0.6 μm/second (Figure 4A). In neurons expressing P50-dynamitin-myc, the average rates of the excursions were diminished compared to controls in all compartments of the neuron. For the cell body, proximal axon, main shaft, and distal axon, the average velocities were 0.21 ± 0.06, 0.23 ± 0.06, 0.16 ± 0.06, and 0.17 ± 0.06 μm/second, respectively (Table 1). Compared to controls, these values represent diminutions of 30, 30, 59 and 56%, respectively (all are statistically different at $p < 0.002$, *t*-test). Figure 4B shows an example from the main shaft. As expected, kymographs of comets from the axons of P50-dynamitin-overexpressing neurons show a steeper slope than kymographs of comets from control axons (Figure 4C). In addition, the kymographs of the P50-dynamitin-overexpressers were more irregular than controls, often showing intermittent patterns corresponding to a lack of detectable motion of the comet between individual frames of the movie.

Graphs of the instantaneous velocities demonstrate that these effects are due to the loss of the more rapid category of instantaneous velocities (Figure 5). Specifically, we found

Table 1: EGFP-EB3 data from control and P50-dynamitin-overexpressing neurons

Category	Condition	Mean velocity (μm/second)	Standard error	# of EGFP-EB3 comets	Total # of measurements
Distal axon	Control	0.39	0.12	19	218
	P50-dynamitin	0.17	0.06	19	253
Axon main shaft	Control	0.39	0.10	24	211
	P50-dynamitin	0.16	0.06	20	238
Proximal axon	Control	0.30	0.10	10	89
	P50-dynamitin	0.23	0.06	19	136
Cell body	Control	0.30	0.10	15	160
	P50-dynamitin	0.21	0.06	19	118

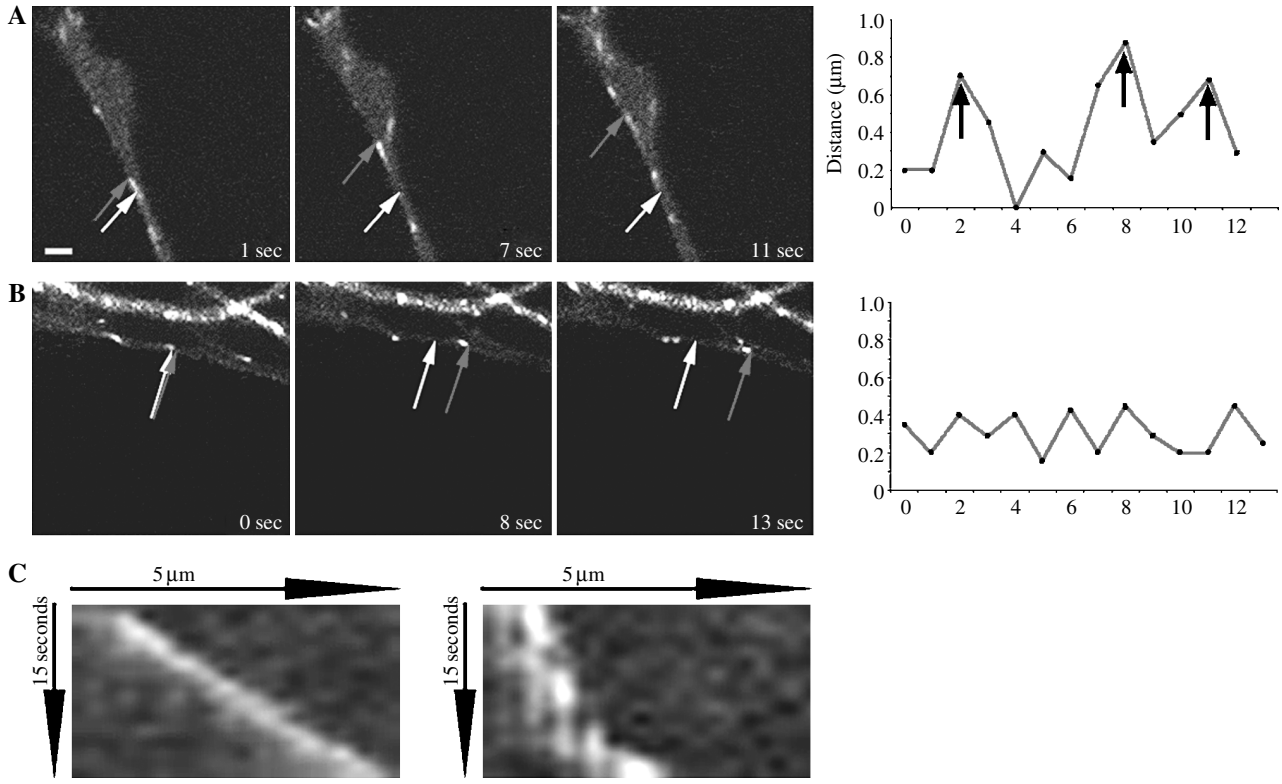

Figure 4: P50-dynamitin overexpression inhibits the fastest instantanous velocities of EGFP-EB3 excursions in short-term neuronal cultures. Shown are still images extracted from time-lapse movies of EGFP-EB3 comets within axons and graphs of data extracted from those movies. In control axons, individual EGFP-EB3 comets were seen to move at instantaneous comet velocities faster than 0.6 μm/s (row A). In axons overexpressing P50-dynamitin, EGFP-EB3 excursions faster than 0.6 μm/s were absent (row B). light and dark arrows in first 3 panels of rows A/B denote initial positions and successive movements of EGFP-EB3 comets, respectively. Arrows in graphs of row A denote instantaneous comet velocities over 0.6 μm/second. Scale bar is 1 μm. (C) Kymographs of comets from the axons of P50-dynamitin-overexpressing neurons (right panel) show a steeper slope than kymographs of comets from control axons (left panel). Kymographs of the P50-dynamitin-overexpressers were more irregular than controls, corresponding to a lack of detectable motion of the comet between individual frames of the movie.

a 97% reduction ($p < 0.001$, chi-square test) in the number of EGFP-EB3 comets with instantaneous velocities above 0.6 μm/second within P50-dynamitin-myc-expressing neurons as compared to control neurons (Figure 5F,G). Duration and directionality of the comets were not significantly different in corresponding compartments of control and experimental neurons (data not shown).

Studies on other cell types have reported a similar diminution in comet velocity in response to dynactin disruption and have attributed it to an effect on microtubule polymerization (25). We reasoned that, if the slowing of the comets were actually caused by a reduction in the transport of the microtubules, the effects on comet velocity should persist over the same timetable as the effects on the transport of short microtubules during the dynactin disruption regime. Moreover, reductions in comet velocity should be observed when DHC is depleted by siRNA. To investigate, we assessed comet velocities in the axons of neurons that had undergone the same re-plating regime as we used for the microtubule transport studies. Neurons overexpressing P50-dynamitin showed EB3 comet velocities that were similar to control neurons [velocity $\pm$ SEM $= 0.149 \pm 0.0049$ μm/second (P50-dynamitin-myc) and 0.157 ± 0.0034 μm/second (control); $p > 0.1$, two-tailed student *t*-test]. In neurons treated with DHC siRNA over a similar timetable, EB3 excursion velocities were increased slightly but significantly (13.7%) when compared to control excursion velocities [velocity $\pm$ SEM $= 0.182 \pm 0.0059$ μm/second (DHC) and 0.157 ± 0.0034 μm/second (control); $p < 0.001$] (Figure 6). This slight increase in the rate of the comets is similar to that observed when actin was disrupted by latrunculin in an earlier study (5) and may relate to a preference for the microtubules to track along other microtubules in the absence of actin and also in the absence of dynein.

In light of these results, there is no evidence of a persistent diminution in comet velocities with either experimental treatment over a similar timetable in which the transport of short microtubules continued to be

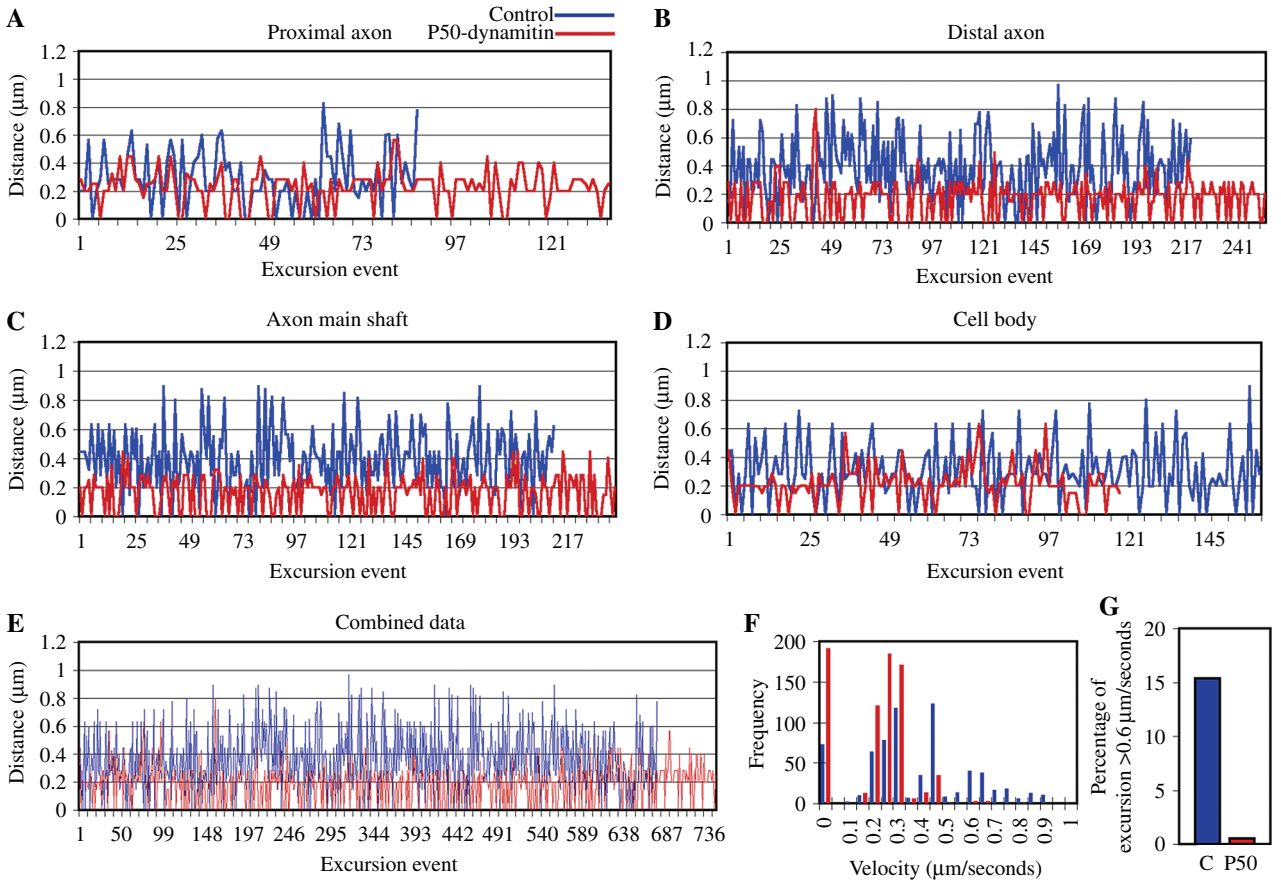

Figure 5: P50-dynamitin overexpression decreases the velocities of EGFP-EB3 excursions in short-term neuronal cultures by selective depletion of fastest instantaneous velocities. In all regions of the axonal shaft (A–C) and within neuronal cell bodies (D), P50-dynamitin overexpression greatly reduced the frequency of EGFP-EB3 comet instantaneous velocities faster than 0.6 μm/second. Blue lines and bars are control data and red lines and bars are experimental (P50-dynamitin-overexpressing cells) data in all graphs. (E) displays axon and cell body data combined, showing the overall differences in instantaneous velocities between controls and P50-dynamitin-overexpressing neurons. (F) is a histogram of all EGFP-EB3 comet instantaneous velocities, clearly displaying a reduction in the frequency of comets moving at velocities above 0.6 μm/second within neurons overexpressing P50-dynamitin (red bars) as compared to control neurons (blue bars). In control neurons, 15.7% of the EGFP-EB3 excursions were faster than 0.6 μm/second, whereas in P50-dynamitin-overexpressing neurons only 0.5% of the EGFP-EB3 excursions were faster than 0.6 μm/second, reflecting a 97% reduction (statistically significant difference; $p < 0.001$, chi square test) in the frequency of fastest comets (G).

compromised. On this basis, we would surmise that comet velocities are particularly fast in freshly plated neurons because of rapid microtubule polymerization rates and that dynactin disruption has a transient effect to diminish these rapid polymerization rates.

Effects of DHC depletion or dynactin disruption on the alignment of microtubules and their invasion into filopodia

One of our most curious findings is the fact that axons grew at fairly normal rates, at least in the culture dish on favorable substrates, when P50-dynamitin was overexpressed or when DHC was depleted, even for a period of days. This was also the case when the treated neurons were re-plated after 1–2 days and allowed to grow axons anew (see earlier). However, when the neurons were re-plated after 3–4 days of DHC depletion, the results were quite different. [Quantitative analyses using Western blotting and immunofluorescence indicate that DHC levels are down by at least 70% by day two after introduction of the siRNA and continue to diminish over days 3 and 4 to 80–90% diminution (6)]. DHC-depleted neurons re-plated after 3–4 days had significantly shorter axons than control neurons, with about 70% diminution of the total axonal length (Figure 7A–C). Immunofluorescence labeling of microtubules and actin filaments revealed that control axons contain a tight bundle of well-aligned microtubules in the axonal shaft (Figure 7D,E). Axonal microtubules became splayed apart in the growth cone, and some of these microtubules invaded filopodia along actin bundles (Figure 7D,E). In DHC-depleted neurons, the microtubule arrays were highly abnormal in the distal regions of the axons (Figure 7F–I), appearing twisted and curled. In fact, in many cases the microtubules crossed one another

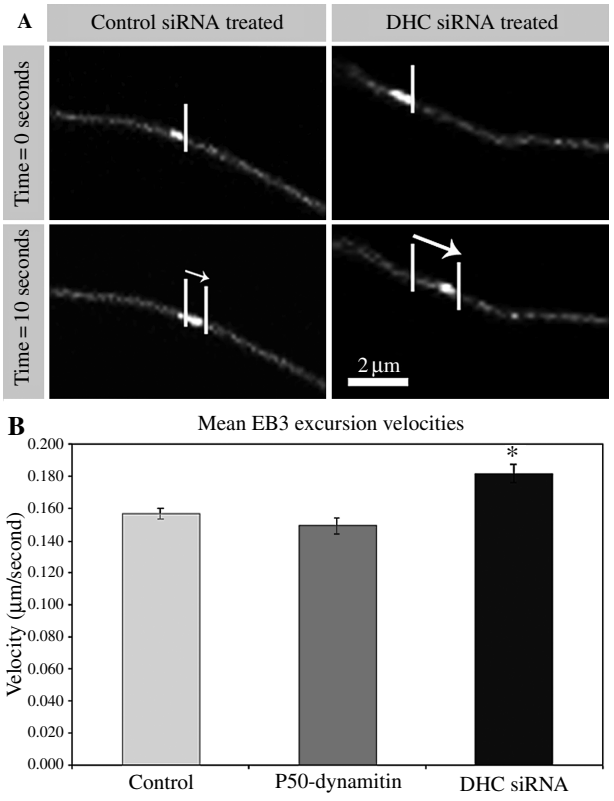

Figure 6: EB3 excursion velocities are not diminished in longer term neuronal cultures by either P50-dynamitin overexpression or DHC siRNA. (A), time-lapse images showing the progression of EB3 comets traveling anterogradely down the axons of either a control-siRNA-treated neuron (left column) or a DHC-siRNA-treated neuron (right column). Positional markers for both time points indicate the progression of EB3 comet excursions. (B), quantification of mean EB3 excursion velocities revealed that, while P50-dynamitin-myc-expressing neurons were indistinguishable from controls (velocity $\pm$ SEM $=$ 0.149 $\pm$ 0.0049 μm/second), DHC siRNA treated cells displayed a slight but significant increase in excursion velocity compared to controls [velocity $\pm$ SEM $=$ 0.182 $\pm$ 0.0059 μm/second (DHC) and 0.157 $\pm$ 0.0034 μm/second (control); two-tailed student *t*-test, *, $p < 0.001$].

in a quilt-like fashion, which presumably indicates an inability of the microtubules to align properly in the absence of cytoplasmic dynein. Unlike in control growth cones where microtubules enter most of the filopodia (Figure 7D), microtubules were completely absent from the filopodia of DHC-depleted growth cones (Figure 7F–I).

With regard to the P50-dynamitin-overexpressing neurons, the distal regions of the axons sometimes displayed similar phenomena, but to a far lesser extent. However, we found that if we exposed these cultures to 16 nM vinblastine to suppress microtubule assembly, we obtained results that were much more reminiscent of those obtained with the DHC depletion regime. With regard to axonal length, the vinblastine treatment alone caused the axons to grow slower, and in combination with the P50-dynamitin, axonal growth was slower yet (see Figure 8 and its legend for statistical details). The morphology and microtubule distribution of the axons treated with vinblastine alone were not dramatically different from controls, but became dramatically different when combined with the P50-dynamitin overexpression. Specifically, the axons were much shorter, thicker and irregularly shaped (many appearing more lamellar than axonal, in that they failed to compress into a cylindrical shape) compared to control axons. In addition, fluorescence images revealed severe abnormalities of the microtubule arrays in these experimental axons (Figure 9). The microtubules in the axons of neurons exposed to vinblastine and excess P50-dynamitin did not form a smooth bundle along the axon, but instead became twisted and disoriented relative to each other (Figure 9, D-D′,E-E′,F-F′). Significantly fewer microtubules invaded filopodia in neurons treated with vinblastine alone (Figure 10A,A′), which is consistent with previous observations on vinblastine-treated neurons [see for example (26)]. The number of microtubules invading filopodia was further reduced in neurons overexpressing P50-dynamitin (Figure 10B,B′). Quantification is shown in Figure 10C.

Discussion

Controversy has surrounded the issue of axonal microtubule transport for decades. The original photobleach studies performed over a decade ago failed to detect movement of axonal microtubules (27,28). Speckle microscopy also failed to detect microtubule movement in the axon (29). The movement of short microtubules down the axon was documented only when the parameters of the photobleach regime were altered so as to detect rapid asynchronous movement as opposed to slow synchronous movement of the microtubules (4). The key to the experimental design is using much longer photobleached zones and much more rapid image acquisition so that rapidly moving fluorescent microtubules can be visualized within the bleached zone. Interestingly, no evidence has yet emerged for any detectable movement of microtubules that exceed a few microns in length. On this basis, we have proposed a 'cut and run' model for axonal microtubule transport, in which long microtubules are essentially immobile and must be cut into short pieces in order to be rapidly transported (30,31). A fundamental tenet of this model is that the molecular motors that transport microtubules are not selective for short microtubules, but rather impinge upon microtubules of all lengths. In this view, long microtubules are still affected by the motor driven forces, but the forces are unable to rapidly transport them.

One goal in the present study was to investigate whether cytoplasmic dynein, a key motor for the anterograde transport of the short microtubules, might also generate 'tugs' of motion on the longer microtubules. Such tugs, if they exist, would not move the long microtubules in a rapid

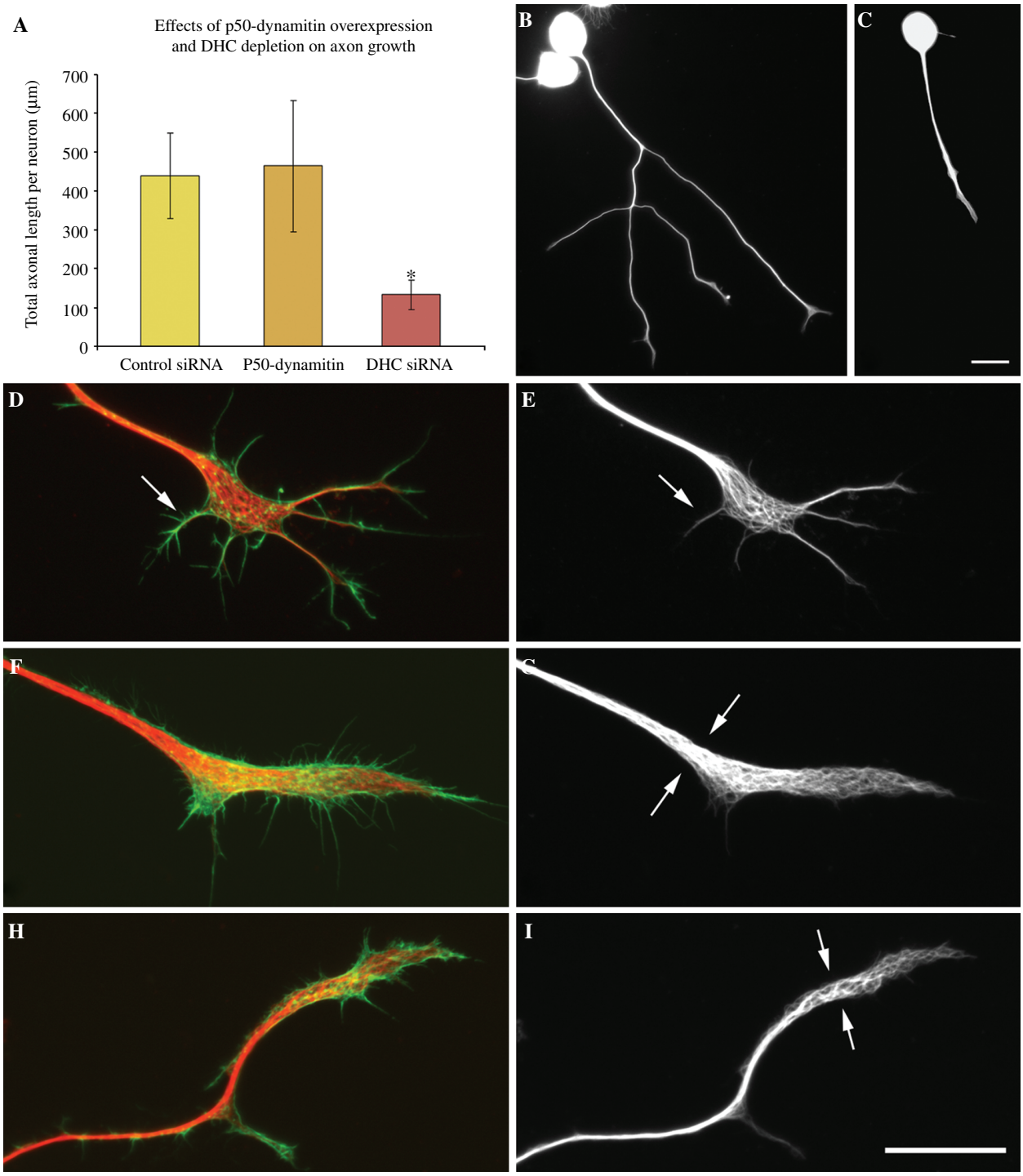

Figure 7: DHC depletion results in stunted axonal outgrowth growth and misalignment of microtubules when neurons are depleted of DHC for 3–4 days and then re-plated. (A), quantification of total axonal length per neuron. There is no significant difference between control and P50-dynamitin-myc-expressing neurons. However, the total axonal length of DHC-depleted neurons is much shorter than that of control neurons, with a 70% decrease in length (*$p < 0.05$, *t*-test). (B and C), low magnification images of microtubule staining of a control neuron and a DHC depleted neuron, respectively. (D–I), high magnification images of growth cones of a control neuron (D and E) and two DHC-depleted neurons (F, G, H and I). In the control growth cone, microtubules form a tight bundle in the axonal shaft, and splay apart in the growth cone. Overlay of microtubule fluorescence image (red) and F-actin fluorescence image (green) (D) reveals microtubules that invade filopodia (arrows in D and E). In DHC-depleted axons, microtubules (G and I) start splaying apart in the distal segment of the axon (arrows) and display marked misalignment and curvature of the microtubules back on themselves. Overlay of microtubules and F-actin reveals that, in contrast to the situation in the control growth cone, virtually no microtubules invade the filopodia of DHC-depleted growth cones (F and H). Scale bars, 20 μm.

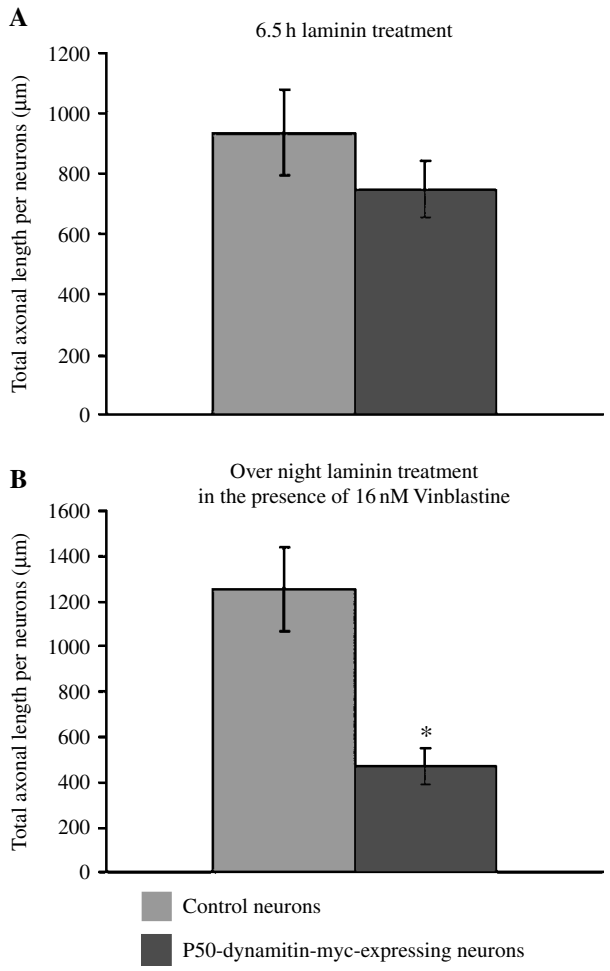

Figure 8: Effects of dynactin disruption on axonal outgrowth: quantification of axonal outgrowth when dynactin is disrupted by P50-dynamitin overexpression, with or without suppression of microtubule dynamics by 16 nM vinblastine (student's *t*-test, two-tailed, *p < 0.05). After exposing the neurons to laminin for 6.5 h, there was a 15% diminution in axonal length comparing controls with P50-dynamitin-overexpressing neurons, but this difference did not meet the criteria of statistical significance. When neurons were exposed to vinblastine, the axonal growth was slowed, such that we had to wait overnight to obtain accurate measurements of axonal length. (Without the vinblastine, overnight was too long because the axons obtained such great lengths, they were impossible to measure). Under these conditions, there was a 60% (statistically significant; student's *t*-test, two-tailed, $p < 0.05$) diminution in axonal length between the axons extended by control neurons, and those extended by P50-dynamitin-overexpressing neurons. Thus, the effects of the two treatments on axonal growth produce a greater effect in combination than they do individually.

concerted fashion, but could theoretically contribute to the advance of the microtubule array down the axon. To test this possibility, we took advantage of the approach recently used by the Popov and Bornens laboratories to study microtubule behaviors in frog axons (9) and migratory cells (23). These authors reasoned that EB 'comets' at the tips of microtubules undergoing assembly move at rates that represent a combination of microtubule polymerization and any potential transport that the microtubule might undergo during the bout of polymerization. In the studies on frog axons, it was concluded that comet velocities are not rapid enough to suggest the transport of microtubules. Even so, it is known that the rates of microtubule transport and polymerization can vary (10), and hence the possibility remained for motors such as cytoplasmic dynein to generate short tugs of motion. To investigate this and related aspects of microtubule organization, we analyzed neurons in which dynactin had been disrupted by overexpression of P50-dynamitin, or within neurons that had been depleted of DHC by siRNA.

Dynactin disruption has recently lost some of its credibility as a reliable method for studying dynein functions because the components of dynactin are now known to interact with other molecular motors as well as non-motor proteins relevant to microtubule behaviors (11,32–34). Nevertheless, our studies indicate that the effects of dynactin disruption are very similar to the effects of DHC depletion on a number of parameters such as Golgi distribution, neurofilament transport and microtubule transport. Therefore, it was initially provocative that an overnight bout of P50-dynamitin overexpression produced a marked diminution in the rates of EB3 comets in the axon. However, this effect was not sustained past the first day of P50-dynamitin overexpression and was not observed in neurons depleted of DHC. In fact, comet rates were actually slightly faster in DHC-depleted growth cones compared to controls. This is particularly noteworthy in light of the fact that the frequency of transport of the short microtubules was compromised in these same axons in which the rates of the EB3 comets were either normal or slightly faster than normal. Thus, we conclude that the transient slowing of the comets during early phases of dynactin disruption is not due to a diminution in polymer movement, but is rather due to a slowing of the rapid rates of microtubule polymerization in these early axons.

If our 'cut and run' model is correct, the long microtubules are subjected to dynein-driven forces, but these forces are unable to overcome the 'drag' on the microtubules that prevents them from undergoing transport. It seems reasonable to posit that such forces might play other roles in the configuration of the microtubules, if not to transport them. Studies from our laboratory suggest that the short microtubules can move either by force generation against other microtubules or against the actin cytoskeleton (5). On this basis, it seems logical to surmise that cytoplasmic dynein might generate forces between long microtubules and other long microtubules as well as between long microtubules and the actin cytoskeleton. A few years ago, we reported that an abrupt disruption of

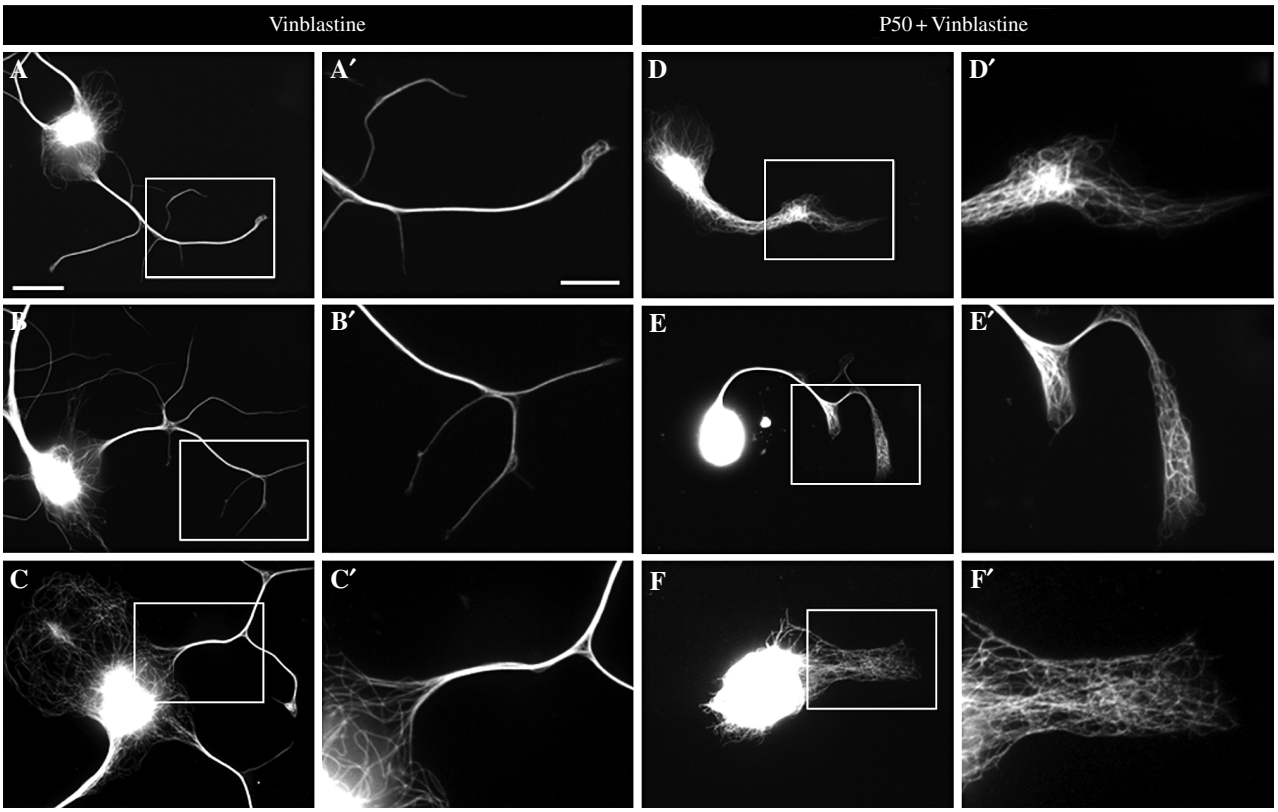

Figure 9: Misalignment of axonal microtubules when microtubule assembly is inhibited and dynactin is also disrupted. (A–C) axonal morphology and microtubule array of dynactin-intact neurons when grown in the presence of 16 nM vinblastine, revealed by β-tubulin immunolabeling. (A′–C′) enlarged images of the enclosed areas in (A–C), revealed smooth, tight microtubule bundles in axons. (D–F) axonal morphology and microtubule array of dynactin-disrupted neurons, by P50-dynamitin overexpression, in the presence of 16 nM vinblastine. (D′–F′) enlarged images of enclosed areas in (D–F), revealed failure to form tight microtubule bundles in the axon, especially in the distal region. Microtubules splayed apart in the axonal shaft and became disoriented relative to each other. Scale bar: (A–C) and (D–F), 20 microns; (A′–C′) and (D′–F′), 10 microns.

dynactin can cause rapid axonal retraction, if the neurons are cultured on a poorly adhesive substrate (35). We suspect that this is because the long microtubules normally interact with the cortical actin via cytoplasmic dynein and that this interaction serves to attenuate the myosin-based contraction of the cortical actin that is responsible for axonal retraction (31).

The experimental approaches utilized in the current study produce more gradual effects and do not cause axons to retract. In fact, and somewhat surprisingly, the axons grow normally during the period of dynactin disruption or dynein depletion. Only when we deplete DHC for 3–4 days and then re-plate do we observe a major defect in the growth rates and morphology of the axon. The dynactin disruption never produces as strong of a phenotype, presumably because it only partially disables the functions of the available dynein motors. With regard to microtubule distribution, the effects are particularly profound in the distal region of the axon, where the microtubules tend to cross over one another in a quilt-like fashion rather than aligning with one another as they normally do in control axons. Even more interestingly, the filopodia of the DHC-depleted growth cones are virtually absent of any microtubules. These observations (and similar observations on dynactin-disrupted neurons treated with vinblastine) are consistent with the idea that dynein-driven forces play major roles in microtubule-microtubule interactions as well as the interactions between microtubules and the actin bundles within filopodia. We believe that these results represent a conservation of the same fundamental mechanisms by which the short microtubules are transported by cytoplasmic dynein against long microtubules or actin. If this is correct, the forces generated by cytoplasmic dynein are likely to be instrumental for the integration of the microtubules and actin bundles during events such as branch formation (36) and growth cone turning (31).

Materials and Methods

Cell culture

Cultures of dissociated neurons from rat superior cervical ganglia were prepared as previously described (37). After dissociation by trituration, the cells were transfected by electroporation (see below) and then plated

in N2 medium at a density of 7500 cells/cm^2 on glass coverslips mounted in the bottom of drilled 35mm diameter plastic Petri dishes whose glass bottoms had been treated for 3h with 0.1 mg/mL poly-D-lysine. All transfections (plasmid and siRNA) were performed directly after dissection and just prior to plating (for details see (6), and below). In some cases, neurons were allowed to grow for either 1-2 or 3-4 days, after which they were detached (0.25% trypsin for 3 minutes), re-plated onto glass-bottom dishes, and allowed to grow axons a second time (38), At least 3h prior to imaging, N2 medium was replaced with pre-warmed L15 plating medium, which has the advantage of maintaining pH in air and auto-fluoresces less than N2 medium. For all culture conditions, medium was supplemented with 25 μg/mL laminin to stimulate rapid outgrowth of axons.

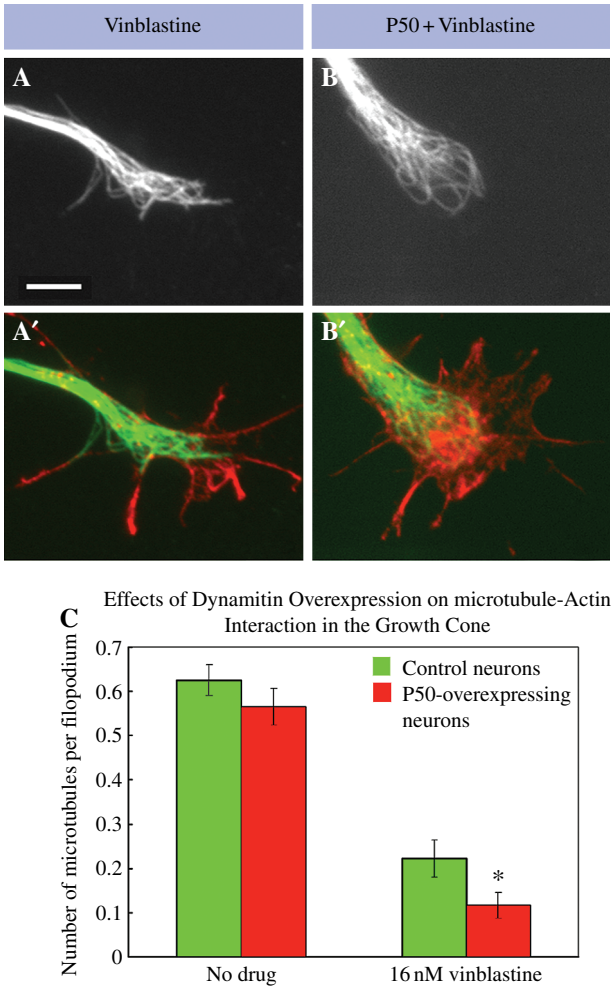

Figure 10: Disruption of dynactin inhibits invasion of microtubules into filopodia when microtubule assembly is inhibited. (A–B) immunostaining of microtubules. (A′–B′) overlay of microtubules (green) and phalloidin-staining of actin (red). In control neurons, microtubules entered the peripheral region of the growth cone, some of which invaded filopodia along actin bundles (see Figure 7). P50-dynamitin overexpressers, microtubule distribution in the growth cone was generally similar to controls (data not shown). In a neuron exposed to 16 nM vinblastine (A and A′), which arrests the assembly of microtubules, fewer microtubules invaded the peripheral region of the growth cone and aligned with the actin bundles. In a P50-dynamitin overexpressing neuron treated with 16 nM vinblastine (B and B′), distal microtubules failed to invade the periphery of the growth cone. (C), analysis of the number of microtubules that entered each filopodium along the actin bundle. Under normal culture conditions, control growth cones and dynactin-disrupted growth cones revealed similar numbers. However, in the presence of 16 nM vinblastine, the number of microtubules that entered each filopodium was much diminished in dynactin-disrupted growth cones relative to that in controls (with vinblastine treatment alone) (*$p < 0.05$, *t*-test, two-tailed). Scale bar, 20 μm.

Transfection of plasmid constructs

A single-cell suspension (at least 1 million cells) of rat sympathetic neurons was pelleted in a tabletop centrifuge at 50.4xg for 3 min and the supernatant was removed with a Pasteur pipette. The cells were re-suspended by gentle trituration in 100 μL of rat Nucleofector Solution (Amaxa Biosystems, Cologne, Germany) and then the total volume was added to plasmid DNA (in sterile water) in a transfection cuvette provided by the manufacturer (Amaxa). All plasmids were added at 10 μg. These plasmids included an EGFP-EB3 plasmid obtained from Niels Galjart (21), an EGFP-α-tubulin plasmid purchased from Clontech and a P50-dynamitin-myc plasmid obtained from Richard Vallee (7). Control plasmids for EGFP and myc were also expressed. Various combinations of plasmids were used, depending on the particular experiment. The DNA/cell suspension was mixed by gently shaking the cuvette, which was then placed in the chamber of the Nucleofection device (Amaxa). Cells were transfected using the manufacturer's recommended settings for primary rat neurons. Immediately following Nucleofection, the cell suspension was transferred to warm N2 medium, and neurons were plated on poly D-lysine-coated glass as explained above.

Live-cell imaging

All the imaging was performed using an AxioVert 200 M inverted microscope (Carl Zeiss, Thornwood, NY, USA) coupled either to an Orca-ER or an Orca II-ER Digital CCD Camera (Hamamatsu, Hamamatsu City, Japan). The CCD camera and most aspects of the microscope were controlled by Axiovision version 3.0 or 4.1 software (Zeiss) running on either a Pentium II based computer (Tekgraf) with the Windows 2000 operating system (Microsoft Corp., Redmond, WA, USA) or an Intel Xeon processor based computer (Fujitsu Siemens, Tokyo, Japan) with the Windows XP Professional operating system (Microsoft Corp.). Images were obtained using a 100X Plan-Neofluar/1.3 NA or a 100X/1.3NA Plan Apo oil immersion objective (Zeiss). Temperature of the cultures was maintained at 37 °C with the use of a Tempcontrol 37–2 digital heated stage and controller, and a Tempcontrol-mini heated objective lens collar and controller (Zeiss). Excitation of fluorescent molecules and collection of correct emission wavelengths were accomplished with an AttoArc 2 or FluoArc Variable Intensity HBO 100 Arc Lamp Control (Atto Instruments, Rockville, MD, USA), a 100 W mercury vapor lamp and the appropriate excitation and emission filters and dichroic mirrors (Chroma, Vermont). To acquire images for live-cell time-lapse movies, neutral density filters were placed in the illuminating light path or the output of the variable intensity mercury lamp was adjusted to reduce photobleaching and photodamage of the sample.

Microtubule transport assay

Sympathetic neurons were transfected with EGFP-tubulin and either a myc-tagged plasmid or a P50-dynamitin-myc construct and cultured as described earlier. Re-plating was performed on day 2. Sixteen to 32 h after re-plating the microtubule transport assay was performed essentially as previously described (5), except that the acquisition parameters were set to utilize 1.8-second intervals and 1.2-second exposure times for a total duration of 241 cycles. These settings correspond to real time image acquisitions intervals of 3 seconds and 13.75 min total imaging time per movie. All microtubule transport live-cell imaging was performed using the Orca II-ER Digital CCD camera and Axiovision 4.1 running on an Intel Xeon processor based computer (Fujitsu Siemens) with the Windows XP Professional operating system (Microsoft Corp.) Image acquisition parameters were adjusted in Axiovision 4.1 prior to imaging in order to provide best possible signal to noise ratio under which to observe microtubule transport. Digital gain was adjusted to 2, dynamic range gain set to 1, gain offset adjusted to 0, and the binning was set

at 2 × 2. Immediately after imaging, dishes were fixed in 25% glutaraldehyde and stained for myc expression using antibodies described below. Only those cells identified as strong overexpressers based on fluorescence intensity were chosen for microtubule transport analysis ($n = 20$; 10 control; 10 P50-dynamitin-myc axons). Motion analyses were performed using Axiovision 4.1 and were aided using digital contrast adjustments within the 'image properties' application, while transport velocities were calculated using the 'measure distance' application. Mean transport velocities were calculated for all observed microtubule transport events ($n = 120$). Final processing of all images was done using Adobe Photoshop 7.0 (Adobe Systems, San Jose, CA, USA).

EGFP-EB3 imaging

Experiments were performed either the day after the initial plating of the neurons or after re-plating as described earlier. Images were acquired at a rate of 1/second for EGFP-EB3 time-lapse movies to maximize the amount of information gathered. To maximize the fluorescent signal while minimizing exposure times, the CCD camera was set to 2 × 2 binning, allowing for shorter camera integration times. Frames extracted for still images were exported from Axiovision as TIFF image files and processed in Photoshop (Adobe Corp.). All EGFP-EB3 quantification was performed using the Axiovision 'measure' module. Raw data were processed and graphs/charts were produced using Excel (Microsoft Corp.). For quantitative analysis of the EGFP-EB3 data, we measured instantaneous velocities as distance traversed between images. The mean excursion velocity was calculated as the distance moved by each EGFP-EB3 comet divided by the time that the comet remained visible. Kymographs were generated for individual EB3 comets using the kymograph function in Metamorph version 6.2r6 (Molecular Devices, Downingtown, PA, USA). Kymograph parameters were set to incorporate 15-second excursions using a line width equal to 3 and collecting maximal values across the width.

Pharmacologic experiments

In some experiments, cultures were exposed at the time of plating to 16 nM vinblastine sulfate to dampen microtubule dynamics. For details, see reference (39).

Fluorescence procedures on fixed cells

For the live-cell imaging experiments, postmortem immunostaining with a myc-antibody was necessary to confirm the expression of P50-dynamitin-myc, given that not all neurons expressing the EGFP-EB3 or EGFP-α-tubulin at appropriate levels also expressed P50-dynamitin-myc at sufficient levels. We only used cells strongly expressing P50-dynamitin-myc, as qualitatively assessed in this fashion. Fluorescence microscopy was also used on fixed cultures to obtain information on the distribution of microtubules, actin filaments, neurofilaments and Golgi. For triple label fluorescence microscopy of microtubules, actin filaments and myc-tag, cultures were simultaneously fixed and extracted in a warm solution containing 1×PHEM (60 mM PIPES, 25 mM HEPES, 10 mM EGTA and 2 mM $MgCl_2$, pH 6.9), 4% paraformaldehyde, 0.15% glutaraldehyde, 0.2% TritonX-100 for 15 min at room temperature. Cells were then rinsed extensively in PBS, pH 7.4. To quench glutaraldehyde-related autofluoresence, cultures were treated twice with 10 mg/mL sodium borohydride, 10 min each time. To double label Golgi and myc-tag (or to label myc-tag in the cultures that has been used for live-cell imaging), cultures were fixed in −20 °C methanol for 15 min, followed by extensive rinsing in PBS. To stain for neurofilaments, cultures were fixed in 1× PHEM buffer containing 4% paraformaldehyde and 1% sucrose for 30 min at room temperature, followed by extraction with 0.5% TritonX-100 in PBS for 10 min. Before addition of primary antibodies, all samples were blocked in 10% normal goat serum plus 10 mg/mL BSA in 1× PBS for at least 30 min. All primary antibodies were diluted in 1× PBS and incubated at 4 °C overnight. Samples were rinsed extensively on the next day and reblocked for at least 15 min. All secondary antibodies were diluted in 1× PBS and incubated at 37 °C for 1 h. After extensive rinse in PBS, samples were mounted in a medium that reduces photobleaching (0.212% N-propylgallate in 90% glycerol and 10% PBS).

Both monoclonal and polyclonal myc-tag antibodies were obtained from Upstate and were used at 1:200 dilution. The monoclonal β-tubulin antibody (Sigma, Milwaukee, WI, USA) was used at 1:200 dilution. The monoclonal Golgi-58 k protein antibody (Sigma) was used at 1:500 dilution. The polyclonal antibody against neurofilament-L was a generous gift from Dr Virginia Lee (University of Pennsylvania) and used at 1:500 dilution. The Alexa Fluor 488 phalloidin (Molecular Probes, Eugene, OR, USA) was incubated with secondary antibodies and used at 1:40 dilution. The Alexa Fluor 488 conjugated secondary antibodies were from Molecular Probes and used at 1:200 dilution. The Cy3- and Cy5-conjugated secondary antibodies were from Jackson ImmunoResearch and used at 1:200 dilution. Samples stained to reveal neurofilaments were observed on an Axiovert 200 M inverted microscope (Zeiss), and images were acquired using a Roper charge-coupled device containing a back-thinned chip. Quantitative analyses of axon length and neurofilament fluorescence along the length of the axon were performed using the segmented mask procedure (40). Others samples were observed on an Axiovert 200 M inverted microscope (Zeiss), and images were acquired using a charge-coupled device (Orca ER; Hamamatsu), using AxioVision 4.0 software (Zeiss). To reveal the general morphology of sympathetic neurons and quantify total axonal length, fluorescent images were taken with a Plan Apochromat 40×/1.00 oil objective; to reveal Golgi apparatus, microtubules and actin filaments in detail, fluorescent images were taken with a Fluar 100×/1.30 oil objective. Axonal length was measured using the arbitrary curve measuring tool in Axiovision 4.0.

Acknowledgments

This work was supported by NIH grants to PWB and MMB and Tobacco Settlement Funds to PWB from the State of Pennsylvania. FJA is a Foreign Faculty Professor funded by the HEC of Pakistan. TPH is supported by a postdoctoral training grant from the NIH. KAM is supported by a predoctoral NRSA from the NIH. We thank Niels Galjart for the EGFP-EB3 construct, Richard Vallee for the P50-dynamitin-myc construct, Virginia Lee for the neurofilament antibody and Wenqian Yu for advice and assistance.

References

1. Schaefer AW, Kabir N, Forscher P. Filopodia and actin arcs guide the assembly and transport of two populations of microtubules with unique dynamic parameters in neuronal growth cones. J Cell Biol 2002;158:139–152.
2. Baas PW, Ahmad FJ. The plus ends of stable microtubules are the exclusive nucleating structures for microtubules in the axon. J Cell Biol 1992;116:1231–1241.
3. Yu W, Baas PW. Changes in microtubule number and length during axon differentiation. J Neurosci 1994;14:2818–2829.
4. Wang L, Brown A. Rapid movement of microtubules in axons. Curr Biol 2002;12:1496–1501.
5. Hasaka TP, Myers KA, Baas PW. Role of actin filaments in the axonal transport of microtubules. J Neurosci 2004;24:11291–11301.
6. He Y, Frances F, Myers KA, Yu W, Black MM, Baas PW. Role of cytoplasmic dynein in the axonal transport of microtubules and neurofilaments. J Cell Biol 2005;168:697–703.
7. Echeverri CJ, Paschal BM, Vaughan KT, Vallee RB. Molecular characterization of the 50-kD subunit of dynactin reveals function for the complex in chromosome alignment and spindle organization during mitosis. J Cell Biol 1996;132:617–633.
8. Ahmad FJ, Echeverri CJ, Vallee RB, Baas PW. Cytoplasmic dynein and dynactin are required for the transport of microtubules into the axon. J Cell Biol 1998;140:391–401.
9. Ma Y, Shakiryanova D, Vardya I, Popov SV. Quantitative analysis of microtubule transport in growing nerve processes. Curr Biol 2004;14:725–730.
10. Keating TJ, Peloquin JG, Rodionov VI, Momcilovic D, Borisy GG. Microtubule release from the centrosome. Proc Natl Acad Sci USA 1997;94:5078–5083.
11. Schroer TA. Dynactin. Annu Rev Cell Dev Biol 2004;20:759–779.

12. LaMonte BH, Wallace KE, Holloway BA, Shelly SS, Ascano J, Tokito M, Van Winkle T, Howland DS, Holzbaur EL. Disruption of dynein/dynactin inhibits axonal transport in motor neurons causing late-onset progressive degeneration. Neuron 2002;34:715–727.
13. Heerssen HM, Pazyra MF, Segal RA. Dynein motors transport activated Trks to promote survival of target-dependent neurons. Nat Neurosci 2004;7:596–604.
14. Vallee RB, Williams JC, Varma D, Barnhart LE. Dynein: an ancient motor protein involved in multiple modes of transport. J Neurobiol 2004;58:189–200.
15. Ho WC, Allan VJ, Van Meer G, Berger EG, Kreis TE. Reclustering of scattered Golgi elements along microtubules. Eur J Cell Biol 1989;48: 250–263.
16. Burkhardt JK, Echeverri CJ, Nilsson T, Vallee RB. Overexpression of the dynamitin (P50) subunit of the dynactin complex disrupts dynein-dependent maintenance of membrane organelle distribution. J Cell Biol 1997;139:469–484.
17. Wang L, Ho CL, Sun D, Liem RKH, Brown A. Rapid movement of axonal neurofilaments interrupted by prolonged pauses. Nat Cell Biol 2000;2:137–141.
18. Roy S, Coffee P, Smith G, Liem RKH, Brady ST, Black MM. Neurofilaments are transported rapidly but intermittently in axons: implications for slow axonal transport. J Neurosci 2000;20:6849–6861.
19. Francis F, Roy S, Brady ST, Black MM. Transport of neurofilaments in growing axons requires microtubules but not actin filaments. J Neurosci Res 2005;79:442–450.
20. Helfand BT, Loomis P, Yoon M, Goldman RD. Rapid transport of neural intermediate filament protein. J Cell Sci 2003;116:2345–2359.
21. Stepanova T, Slemmer J, Hoogenraad CC, Lansbergen G, Dortland B, De Zeeuw CI, Grosveld F, van Cappellen G, Akhmanova A, Galjart N. Visualization of microtubule growth in cultured neurons via the use of EB3-GFP (End-Binding Protein 3-Green Fluorescent Protein). J Neurosci 2003;23:2655–2664.
22. Vaughan KT. Surfing, regulating and capturing: are all microtubule-tip-tracking proteins created equal? Trends Cell Biol 2004;14: 491–496.
23. Abal M, Piel M, Bouckson-Castaing V, Mogensen M, Sibarita JB, Bornens M. Microtubule release from the centrosome in migrating cells. J Cell Biol 2002;159:731–737.
24. Baas PW, White LA, Heidemann SR. Microtubule polarity reversal accompanies regrowth of amputated neurites. Proc Natl Acad Sci USA 1987;84:5272–5276.
25. Piehl M, Cassimeris L. Organization and dynamics of growing microtubule plus ends during early mitosis. Mol Biol Cell 2003;14:916–925.
26. Suter DM, Schaefer AW, Forscher P. Microtubule dynamics are necessary for SRC family kinase-dependent growth cone steering. Curr Biol 2004;14:1194–1199.
27. Lim SS, Edson KJ, Letourneau PC, Borisy GG. A test of microtubule translocation during neurite elongation. J Cell Biol 1990;111:123–130.
28. Hirokawa N, Terada S, Funakoshi T, Tekeda S. Slow axonal transport: the subunit transport model. Trends Cell Biol 1997;7:384–388.
29. Chang S, Svitkina TM, Borisy GG, Popov SV. Speckle microscopic evaluation of microtubule transport in growing nerve processes. Nat Cell Biol 1999;7:399–403.
30. Baas PW, Karabay A, Qiang L. Microtubules cut and run. Trends Cell Biol 2005;15:518–524.
31. Baas PW, Nadar CV, Myers KA. Axonal microtubule transport: the long and short of it. Traffic 2006 (in press).
32. Deacon SW, Serpinskaya AS, Vaughan PS, Lopez-Fanarraga M, Vernos I, Vaughan KT, Gelfand VI. Dynactin is required for bidirectional organelle transport. J Cell Biol 2003;160:297–301.
33. Gross SP. Dynactin: coordinating motors with opposite inclinations. Curr Biol 2003;13:R320–R322.
34. Carvalho P, Gupta ML, Hoyt MA, Pellman D. Cell cycle control of kinesin-mediated transport of Bik1 (CLIP-170) regulates microtubule stability and dynein activation. Dev Cell 2004;6:815–829.
35. Ahmad FJ, Hughey J, Wittmann T, Hyman A, Greaser M, Baas PW. Motor proteins regulate force interactions between microtubules and microfilaments in the axon. Nat Cell Biol 2000;2:276–280.
36. Dent EW, Kalil K. Axon branching requires interactions between dynamic microtubules and actin filaments. J Neurosci 2001;21: 9757–9769.
37. He Y, Baas PW. Growing and working with peripheral neurons. Methods Cell Biol 2003;71:17–35.
38. Karabay A, Yu W, Solowska JM, Baird DH, Baas PW. Axonal growth is sensitive to the levels of katanin, a protein that severs microtubules. J Neurosci 2004;24:5778–5788.
39. Baas PW, Ahmad FJ. The transport properties of axonal microtubules establish their polarity orientation. J Cell Biol 1993;120:1427–1437.
40. Brown A, Slaughter T, Black MM. Newly assembled microtubules are concentrated in the proximal and distal regions of growing axons. J Cell Biol 1992;119:867–882.